Electronic Supplementary Information for

Design of PDMS/PAN Composite Membranes with Ultra-Interfacial Stability *via* Layer Integration

Chao Sang,[a] Siyuan Zhang,[b] Zhihao Si,[a] Qinxu Li,[a] Hanzhu Wu,[a] Lankun Wang,[a] Shilong Dong,[a] Jan Baeyens,[c] Peng-Fei Cao*[d] and Peiyong Qin*[a]*

[a] National Energy R&D Center for Biorefinery, College of Life Science and Technology, Beijing University of Chemical Technology, Beijing, 100029, P. R. China.

[b] Tianjin Key Laboratory of Molecular Optoelectronic Sciences, Department of Chemistry, School of Science, Tianjin University, Tianjin, 300072, P. R. China.

[c] Department of Chemical Engineering, KU Leuven, 2860 Sint-Katelijne-Waver, Belgium

[d] State Key Laboratory of Organic-Inorganic Composites, Beijing University of Chemical Technology, Beijing, 100029, P. R. China.

Corresponding Authors:

Z. Si: zhsi@mail.buct.edu.cn;

P. Cao: caopf@buct.edu.cn;

P. Qin: qinpeiyong@tsinghua.org.cn.

Content

1. Materials

Methanol (MeOH, 99%) and KH570 (97%) were obtained by Aladdin Co., Ltd, China. PDMS (5000 cP) was obtained from Shandong Dayi Chemical, China. GMA, (97%), *n*-heptane (98%), ethyl acetate (99%), 2-hydroxy-2-methylpropiophenone (98%), dibutyltin dilaurate (96%), tetrahydrofuran (98%) and NaOH (98%) were obtained from Macklin Co. Ltd., China. Phenol (99%) was purchased from Sigma-Aldrich. PAN substrate (LJPAN-01) was obtained by Lanjing membrane engineering Co., Ltd., China.

2. Modification of PAN substrates

The NaOH modification time of the PAN substrates is 2 min, and then modified in 0.03 M GMA/MeOH solution for 3 h.

3. Fabrication of PDMS/PAN composite membranes

PDMS, *n*-heptane, KH570 and dibutyltin dilaurate were mixed at a mass ratio of 11: 25: 0.075: 0.05, and stirred for 24 h at room temperature. Subsequently, 2-hydroxy-2-methyl-propiophenone was added into the coating solution and stirred for 30 min. Then, the mixture was coated on the PAN substrate by Elcometer 4340 coater. Then the liquid layer was irradiated under UV lamp (365 nm, 165 mW cm^{-2}). The fabrication methods of PDMS-0.06 and PDMS-0.09 are the same as above.

4. Characterization methods

FT-IR spectra of PAN substrates were determined by an iS10 spectrometer (Nicolet, USA). Solid State ^{1}H-NMR of PAN substrates were using a JNM-ECZ600R (JEOL, Japan). A ESCALAB 250Xi spectrometer (Thermo Fisher Scientific, USA) was employed to perform the X-ray photoelectron spectroscopy of PDMS/PAN and PDMS/GPAN-1. The water contact angles on PAN substrates were determined with JC2000D3 (Shanghai Zhongchen Corporation, China). SEM (SU1510 Hitachi, JEOL Ltd, Japan) was used to observe the morphology and cross-section of PDMS/PAN composite membranes. The nano-scratch examination of the PDMS/PAN membrane surface was conducted on the Nst^{3} (Anton Paar, Austria). The applied load gradually increased from the initial 3 mN to a maximum of 60 mN, with an increase rate of 57 mN min^{-1}. The thermal stability of PDMS/PAN and PDMS/GPAN-1 were investigated by thermos-gravimetric analysis (NETZSCH STA449F5 Jupiter, Germany) under nitrogen atmosphere with a heating rate of 10 °C min^{-1} from room temperature to 800 °C. Differential scanning calorimeter (NETZSCH DSC214, Germany) was carried out under N_2 atmosphere

with a heating rate of 10 °C min^{-1} from -80 °C to 500 °C, then hold at 500 °C for 5 min and cooled from 500 °C to -80 °C at 10 °C min^{-1}. Friction experiments were conducted on a self-designed device as shown in **Movie S2.** Place a 1 kg weight on a 400 mesh sponge gauze and rub the surface of the composite membrane at a speed of 1 cm s^{-1}. The composite membrane was soaked in solvent for 96 h to evaluate the swelling characteristics of the PDMS separation layer. The swelling degree (wt%) was determined according to the calculation method of Wan et al.[1] Real-time infrared spectroscopy was determined on Nicolet 5700 equipment. The DBC was calculated as follows:

$$DBC(\%) = \frac{S_0 - S_t}{S_0} \times 100\% \quad (1)$$

where S_0 and S_t are the peak areas at 0 s and t s, respectively.

5. PV performance evaluation

The PV performance evaluation setup was as described in our previous work[2]. The phenol feed concentration was 1000 ppm. The choice of feed concentration (1000 ppm) comes from some practical application scenarios. For example, it is reported that phenol wastewater from coking plant generally has a concentration of 600-1200 ppm[3]; phenol wastewater from paper mill generally has a concentration of 1000-1800 ppm[4]. The analysis of phenol concentrations in feed and permeate were conducted by Shimadzu GC-14C gas chromatograph. The total flux (J, g m^{-2} h^{-1}) and separation factor (β) were calculated as follows:

$$J = \frac{W}{A \times t} \quad (2)$$

$$\beta = \frac{y_{b/(1-y_b)}}{x_{b/(1-x_b)}} \quad (3)$$

where A (m^2), t (h), and W (g) represents the membrane area, the test time, and the permeate mass; y_b and x_b are the permeate and feed concentrations of phenol, respectively.

6. PV stability test

During PV test, the membrane module was connected to the feed tank, and the feed solution was circulated using a peristaltic pump. The phenol concentration in water was maintained at 20 wt%, and the feed temperature was set at 80 ℃ throughout the PV process. The entire experimental duration was 72 h to assess membrane durability. PV was interrupted 3 times, and the membrane module was removed to evaluate its recyclability.

7. Gas transport measurement

The carbon dioxide, hydrogen, helium, methane and nitrogen permeability were measured at 25 °C and 1 bar based on previous work.[5] The permeability performance was evaluated by single gas steady-state permeation rate (P) and the ideal selectivity ($\alpha_{A/B}$) as follows:

$$P = \frac{273 \times 10^{10}}{760} \frac{VL}{AT\left(\frac{P2 \times 76}{14.7}\right)} \frac{dp}{dt} \quad (4)$$

$$\alpha_{A/B} = \frac{p_A}{P_B} \quad (5)$$

where V and L are the volume (cm^3) of the downstream chamber and membrane thickness (cm), respectively. A and T refer to the effective area of the membrane (cm^2) and the experimental temperature (K) respectively. $p2$ (psia) is the pressure of the feed gas in the upstream chamber.

8. MD simulation

The PDMS/PAN membrane fragment was modeled utilizing semi-empirical DFT calculation under PM6D3 level. Force field parameters were generated based on the PAN chain amber force field or Hessian matrix. In a cubic cell with a side length of 6 nm, this fragment solvated by water was subjected to a 200 ps MD simulation under the NVT ensemble, whose temperature was controlled at 333.15 K. The MD trajectory is used to calculate MSD, whose first derivative with time is exactly proportional to the diffusion coefficient. A simulation lasting of 2 ns was conducted with a gradient of phenol concentration. The force field parameters were fitted using the Sobtop program based on DFT calculations with the Gaussian09 program. During the entire simulation process, a constant acceleration is applied to the Si atoms in the PDMS layer to simulate the impact force on the membrane during the actual separation process.

9. Tables and Figures

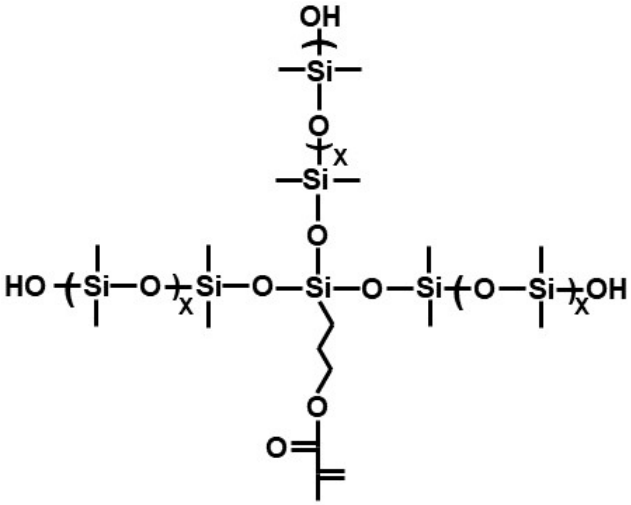

Fig. S1. The structural formula of methacrylate-PDMS.

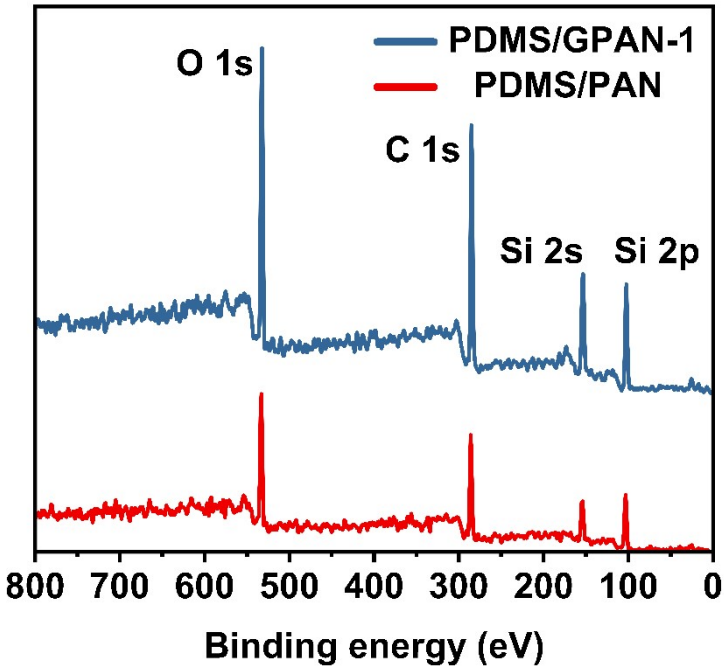

Fig. S2. X-ray photoelectron spectroscopy spectra of PDMS/PAN and PDMS/GPAN-1.

Fig. S3. The digital image of PDMS/GPAN-1.

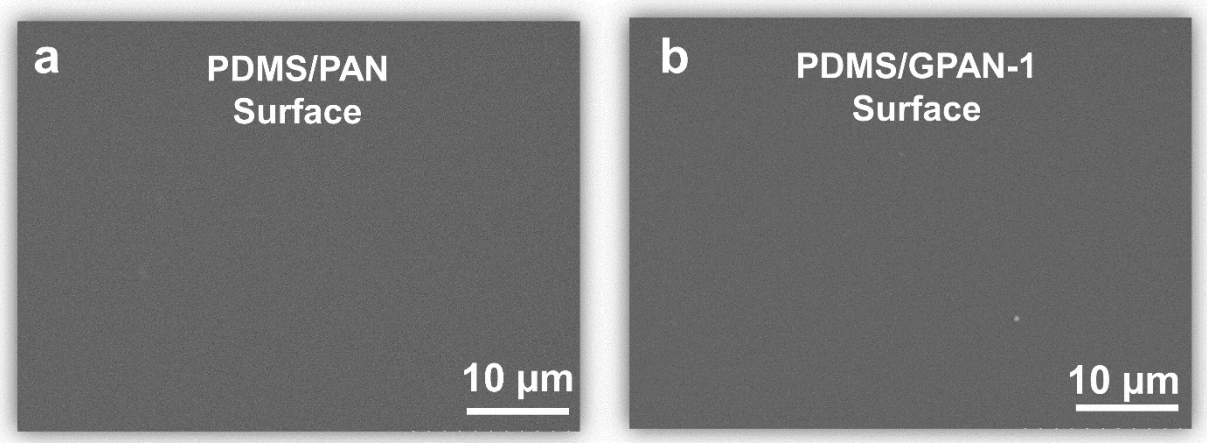

Fig. S4. SEM micrographs of the membrane surface for (a) PDMS/PAN and (b) PDMS/GPAN-1.

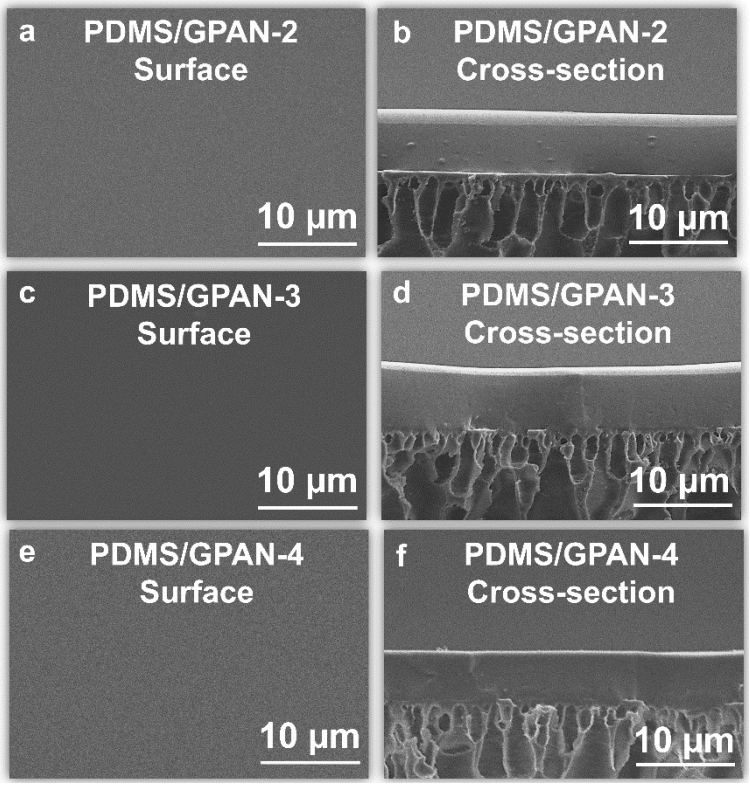

Fig. S5. SEM micrographs of the membranes (a) surface and (b) cross-section for PDMS/GPAN-2, (c) surface and (d) cross-section for PDMS/GPAN-3 and (e) surface and (f) cross-section for PDMS/GPAN-4.

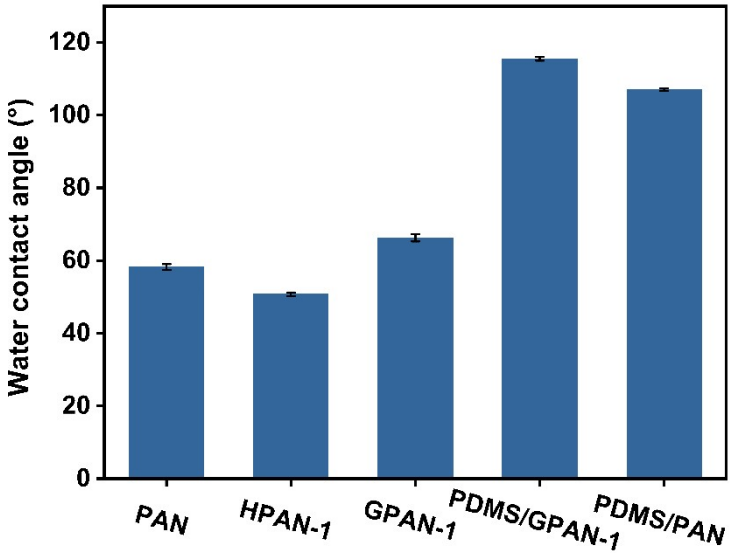

Fig. S6. Water contact angles of PAN, HPAN-1, GPAN-1, PDMS/GPAN-1 and PDMS/PAN.

The water contact angle of HPAN-1 decreases from 58.25° of PAN to 50.75° due to the presence of hydrophilic aminogroups[6]. Further, the water contact angle of GPAN-1 increases to 66.25° because of the introduction of acrylate groups[7]. Furthermore, PDMS/GPAN-1 suggests a high value of 115.5°, significantly higher than GPAN-1. This is because of the hydrophobic coating of PDMS covering GPAN-1. PDMS/PAN has a slightly lower value than PDMS/GPAN-1 due to its low solid surface tension caused by poor interfacial interactions[8].

Table S1: Nano-scratch test results of different polymeric membranes.

Membrane	Selective layer thickness (μm)	Substrate	Critical load (mN)	Ref.
PDMS	5	Hollow fiber ceramic	17	9
PDMS	7	Hollow fiber ceramic	27	9
PDMS	6	Tubular ceramic	24	9
PDMS	9	Tubular ceramic	30	9
PDMS	6	PVDF	16.3	10
PDMS	9	PVDF	33.2	10
PDMS	5.5	Tubular ceramic	29.2	11
PDMS	6	Tubular ceramic	28.3	11
PDMS	6.5	Tubular ceramic	27.4	11
PDMS	10	Hollow fiber ceramic	32	12
PDMS	4.7	PVDF	16	13
GO[a]	1.5	Hollow fiber ceramic	30.62	14
PDMS	10	Tubular ceramic	27.6	15
PEBA[b]	6	Hollow fiber ceramic	18.9	16
PDMS/GPAN-1	7	PAN	45.73	this work

a): Graphene oxide

b): Poly(ether-block-amide).

Table S2: Degree of swelling in a PDMS on unmodified PAN substrate and alternated PAN substrate in *n*-heptane, ethyl acetate, and tetrahydrofuran at 40 °C over a duration of 4 days.

Membrane	*n*-Heptane	Ethyl acetate	Tetrahydrofuran
PDMS/PAN	97.5%	67.6%	31.1%
PDMS/GPAN-1	25.8%	11.6%	6.4%

Table S3. Solubility indices and their discrepancies in solubility indices among polymeric substance and solvent medium.

	δ_d(Mpa$^{1/2}$)	δ_p(Mpa$^{1/2}$)	δ_h(Mpa$^{1/2}$)	$\Delta\delta_{PDMS,j}$[a]	$\Delta\delta_{PAN,j}$[a]
n-Heptane[17]	15.3	0.0	0.0	4.7	21.1
Ethyl acetate[17]	15.8	5.3	7.2	5.8	12.7
Tetrahydrofuran[17]	16.8	5.7	8.0	6.6	12.2
PAN[18]	13.8	16.2	13.5	18.5	—
PDMS[19]	15.9	0.1	4.7	—	18.5

[a] $\Delta\delta_{i,j}$ is calculated by $\triangle \delta_{i,j} = \sqrt{(\delta_{d,i} - \delta_{d,j})^2 + (\delta_{p,i} - \delta_{p,j})^2 + (\delta_{h,i} - \delta_{h,j})^2}$

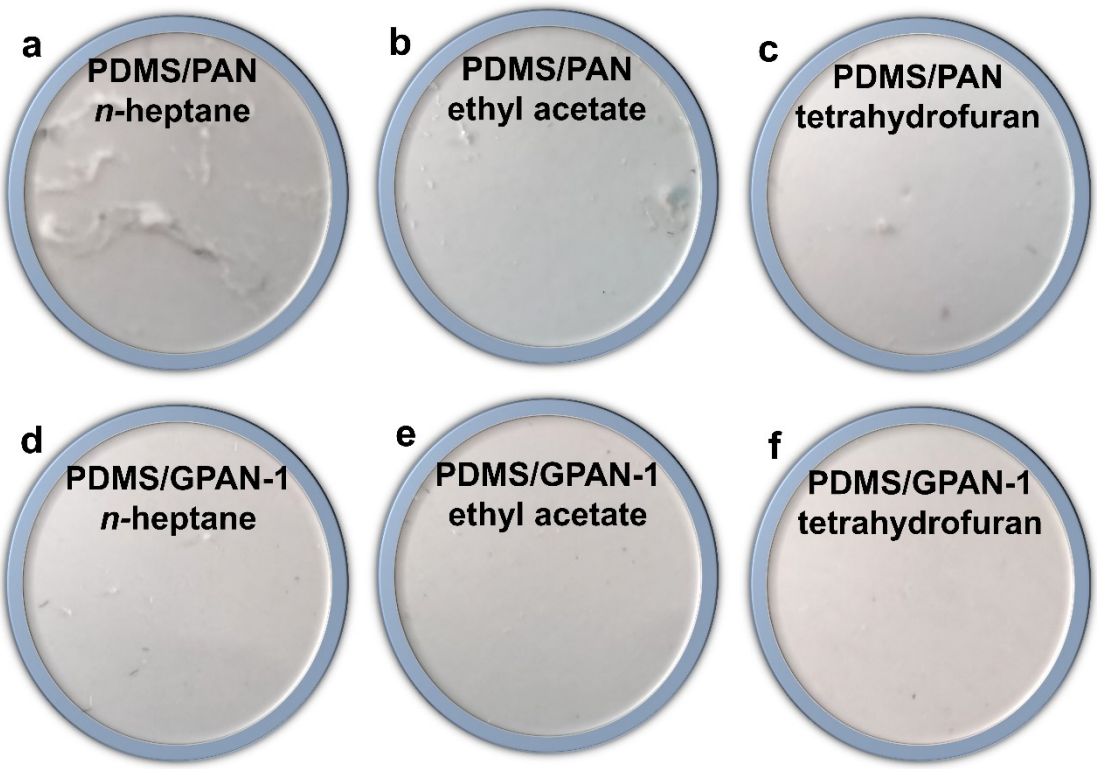

Fig. S7. Digital image of PDMS/PAN surface after swelling test in (a) *n*-heptane, (b) ethyl acetate, and (c) tetrahydrofuran. Digital image of PDMS/GPAN-1 surface after swelling test in (d) *n*-heptane, (e) ethyl acetate, and (f) tetrahydrofuran.

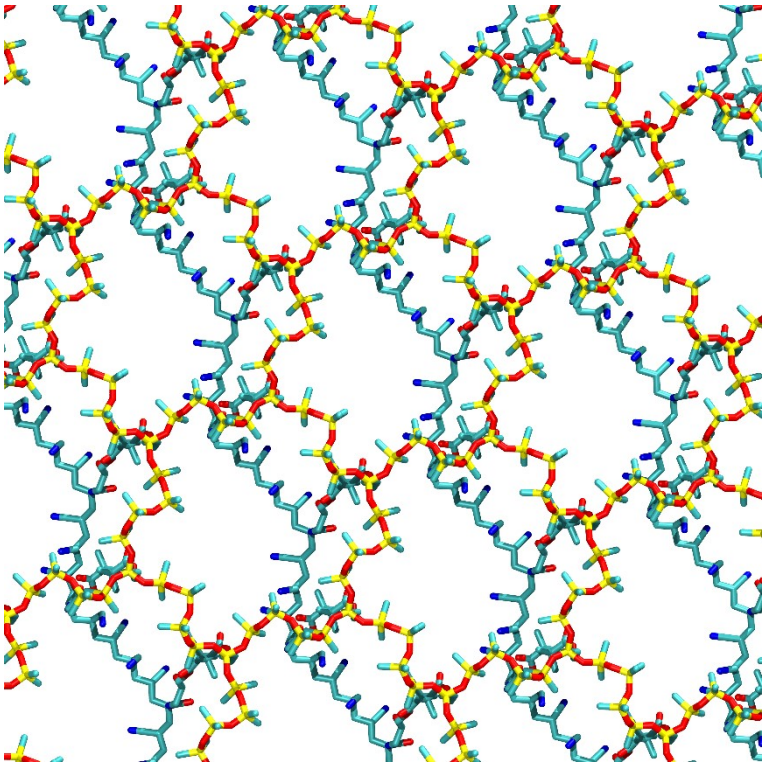

Fig. S8. The two-dimensional network of PDMS.

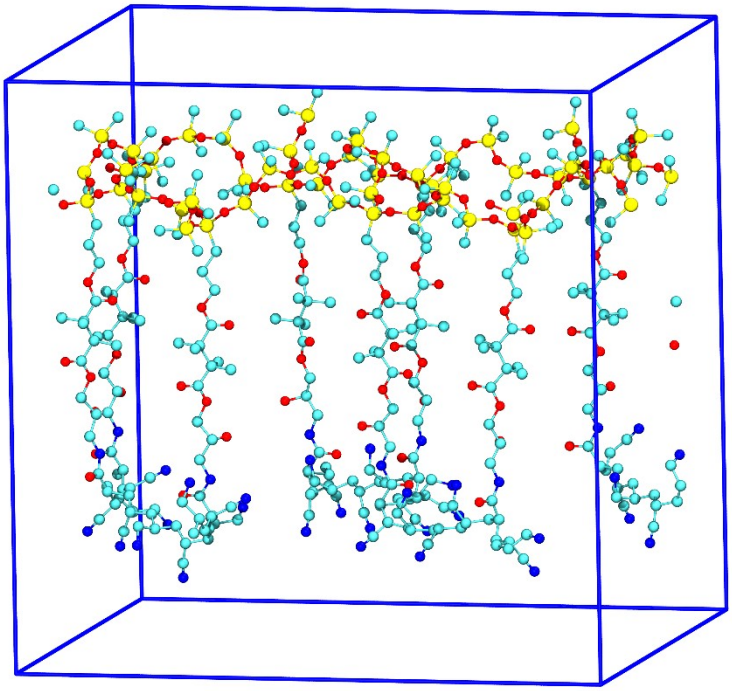

Fig. S9. A full-linked PDMS/PAN model.

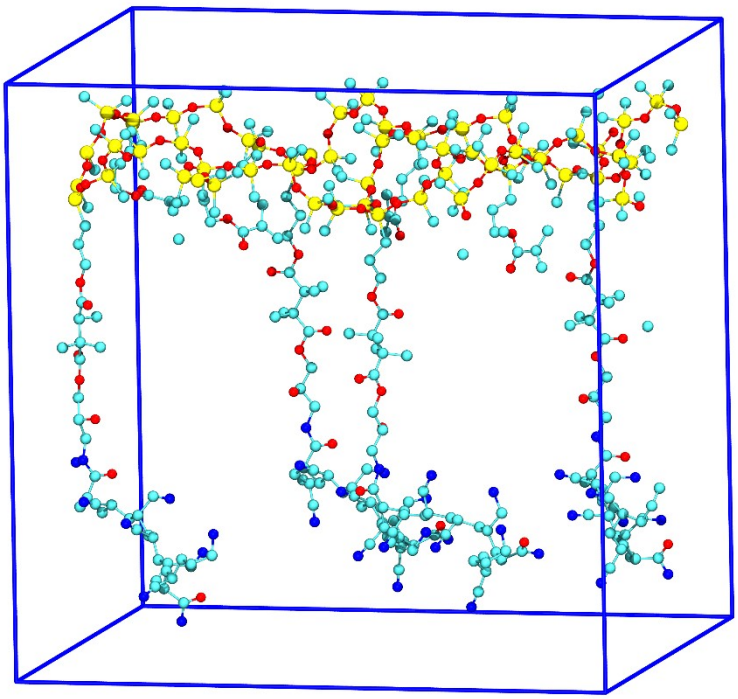

Fig. S10. A half-linked PDMS/PAN model.

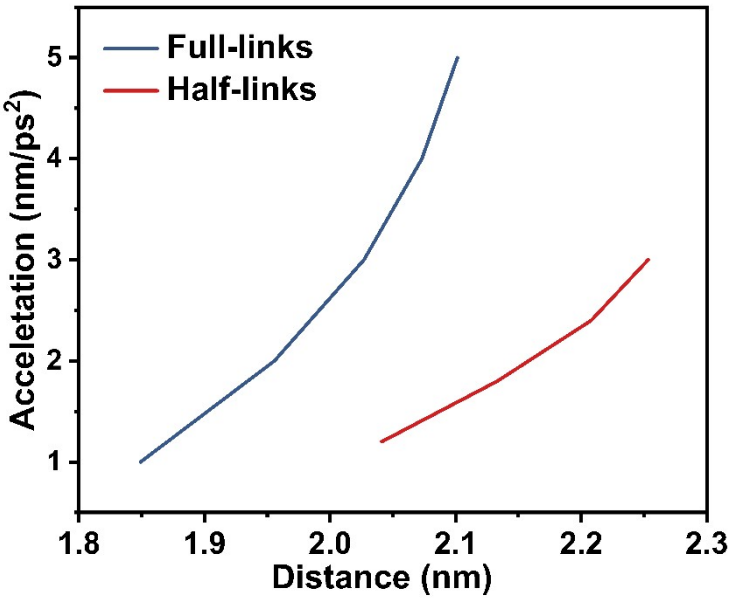

Fig. S11. The stress strain curve of full-links and half-links PDMS/PAN models.

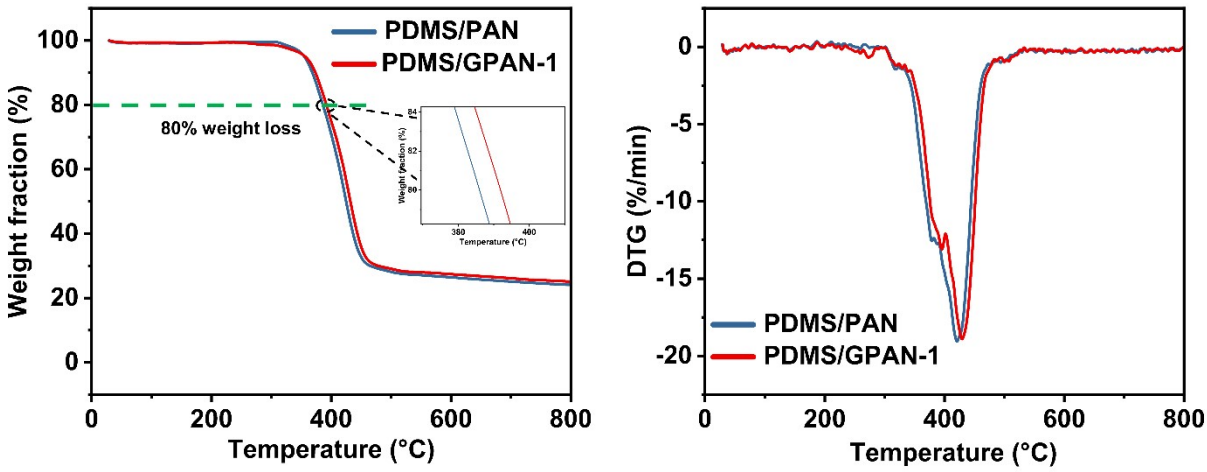

Fig. S12. Thermogravimetric analysis and derivative thermogravimetric curves of PDMS/PAN and PDMS/GPAN-1.

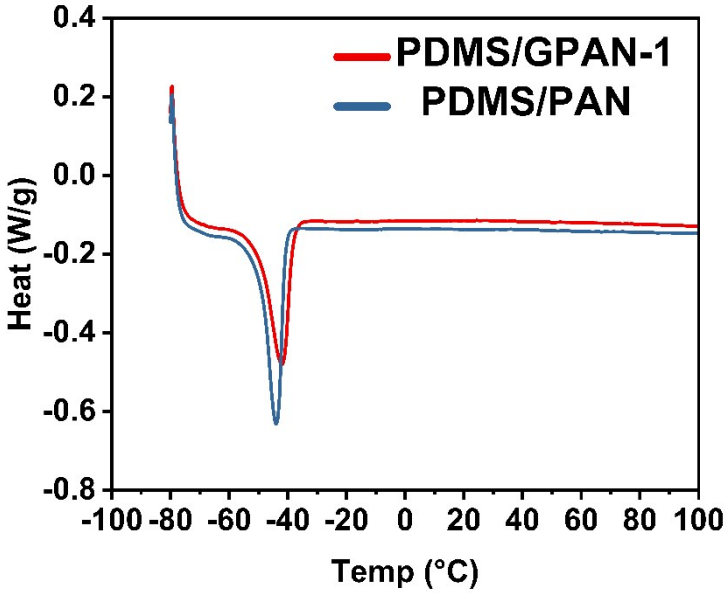

Fig. S13. Differential scanning calorimetry curves of PDMS/PAN and PDMS/GPAN-1.

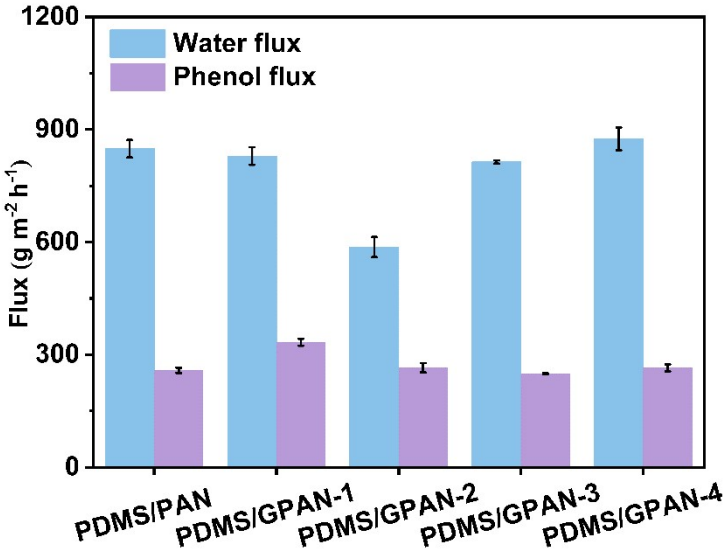

Fig. S14. Effect of NaOH solution concentration used for substrate modification on the phenol flux and water flux of PDMS/PAN composite membranes in the separation of a 1000 ppm phenol-containing aqueous solution at 60 ℃.

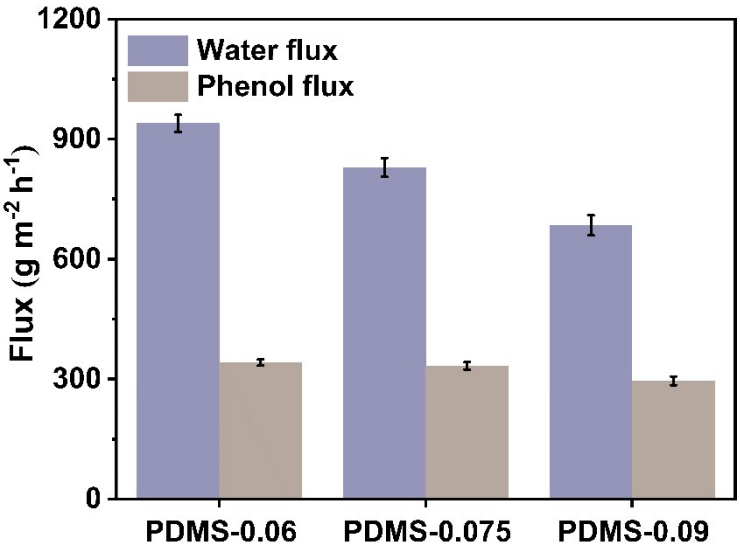

Fig. S15. Influence of KH570 amount on the phenol flux and water flux of PDMS/PAN composite membranes in separating 1000 ppm phenol aqueous solution at 60 ℃.

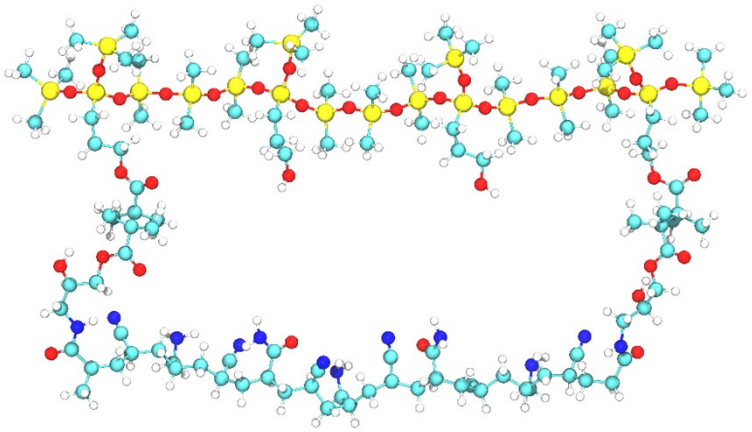

Fig. S16. PDMS/PAN model with 0 covalent bonds between PDMS and PAN layers in MD simulation.

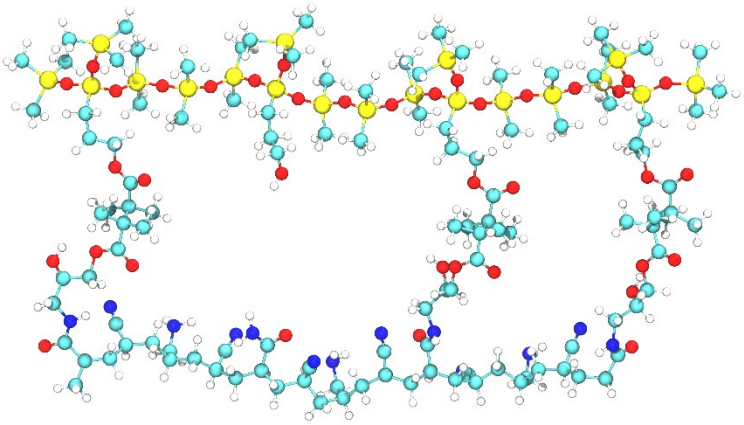

Fig. S17. PDMS/PAN model with 1 covalent bonds between PDMS and PAN layers in MD simulation.

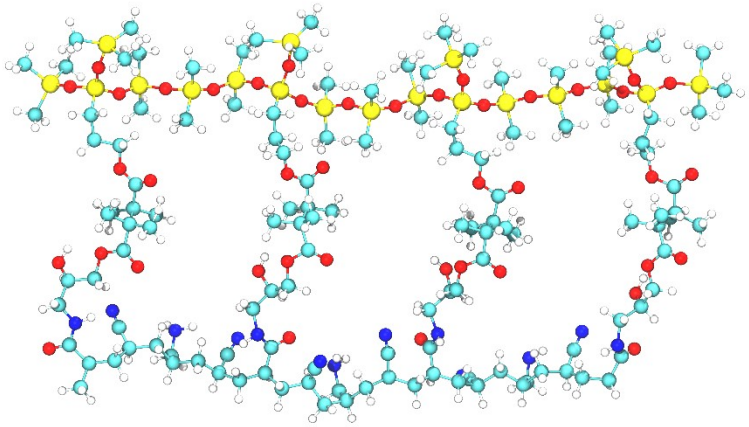

Fig. S18. PDMS/PAN model with 2 covalent bonds between PDMS and PAN layers in MD simulation.

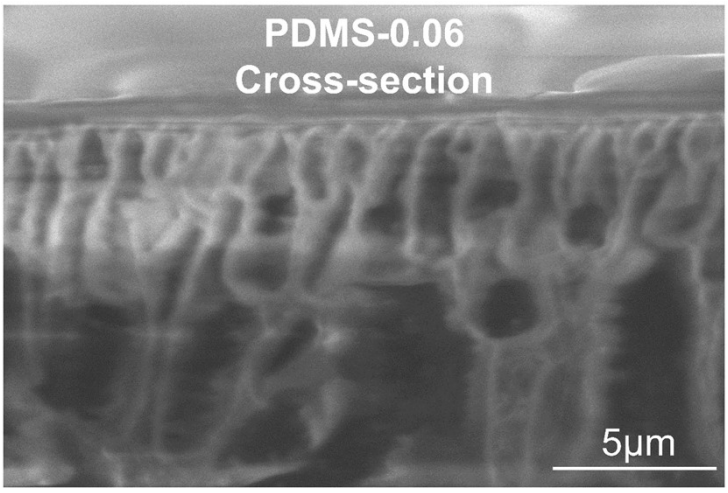

Fig. S19. SEM image of the cross-section of PDMS-0.06.

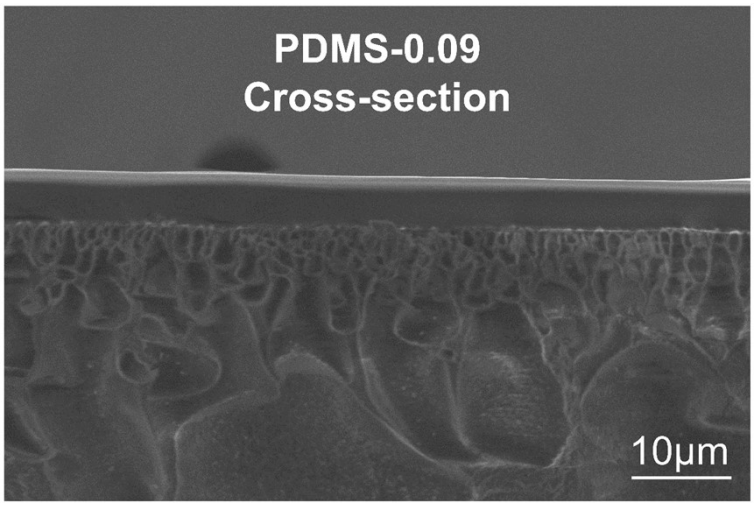

Fig. S20. SEM image of the cross-section of PDMS-0.09.

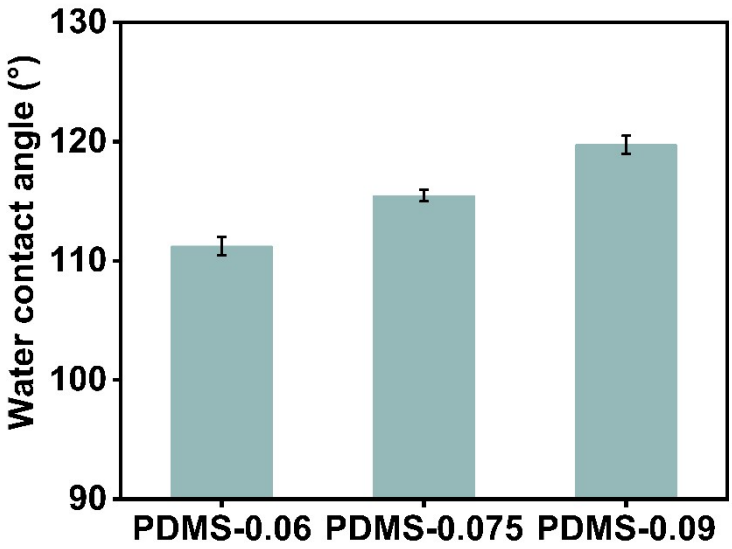

Fig. S21. Water contact angles of PDMS-0.06, PDMS-0.075 and PDMS-0.09.

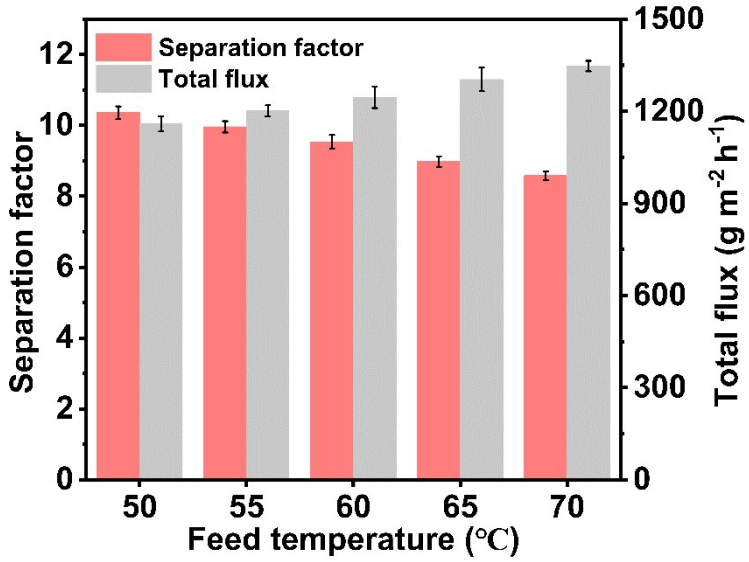

Fig. S22. PV of PDMS/GPAN-1 in different feed temperature.

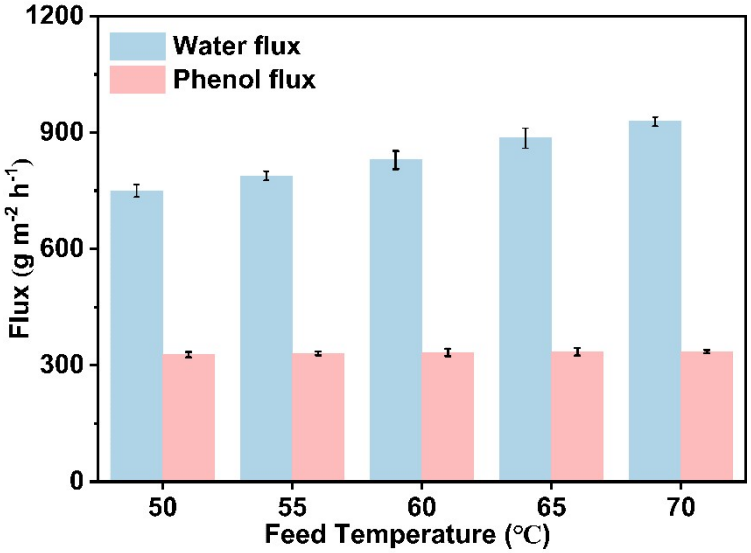

Fig. S23. The phenol flux and water flux of PDMS/GPAN-1 in different feed temperature.

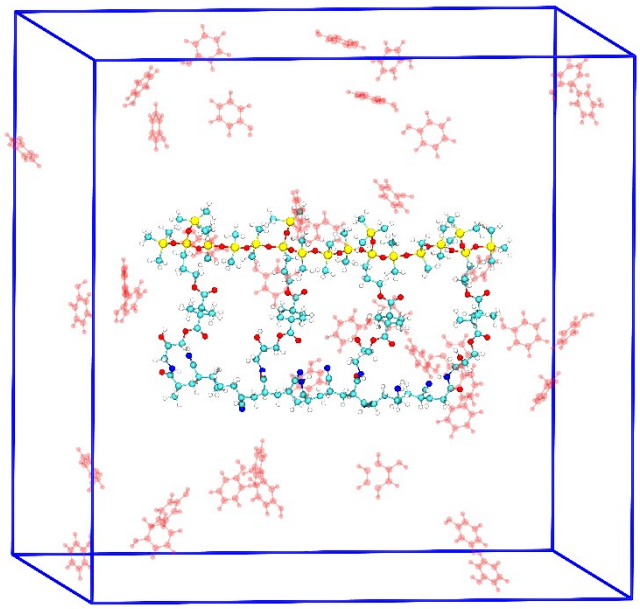

Fig. S24. The initial state of phenol adsorption at 3 wt% concentrations.

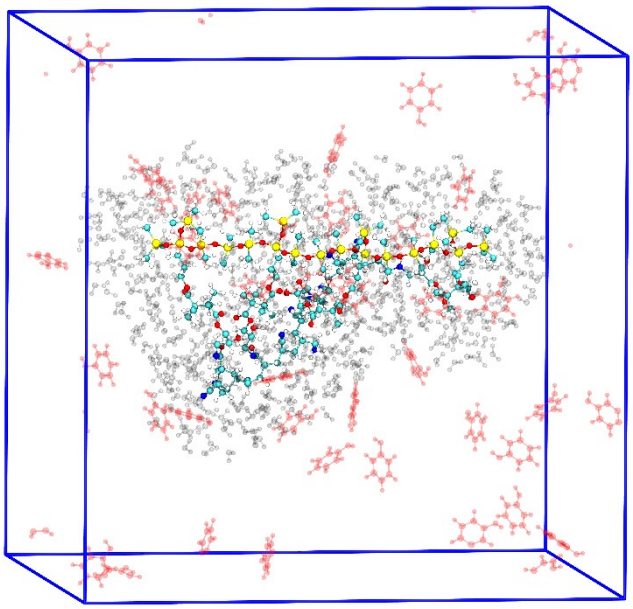

Fig. S25. The termination state of phenol adsorption at 3 wt% concentrations.

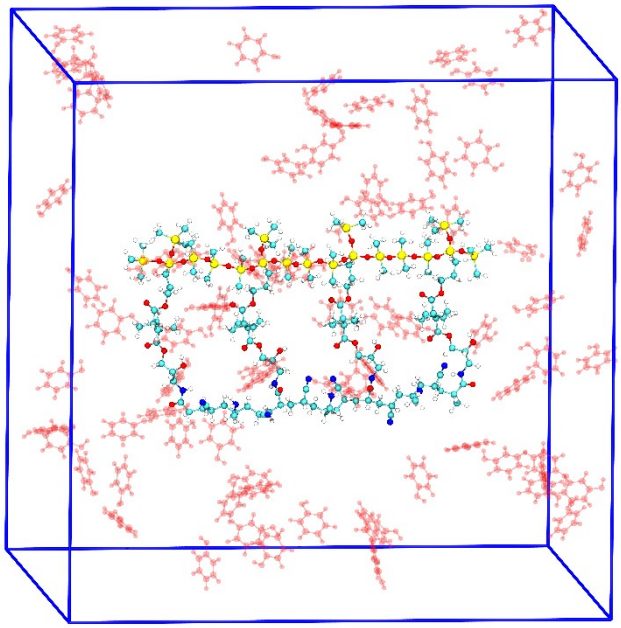

Fig. S26. The initial state of phenol adsorption at 6 wt% concentrations.

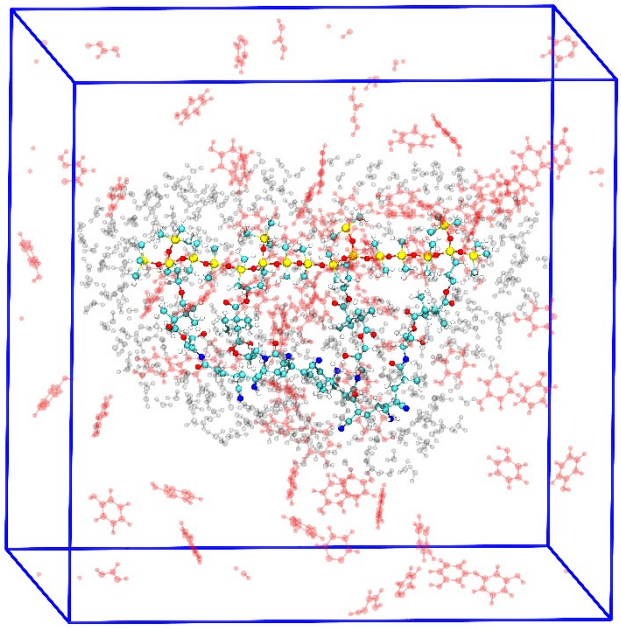

Fig. S27. The termination state of phenol adsorption at 6 wt% concentrations.

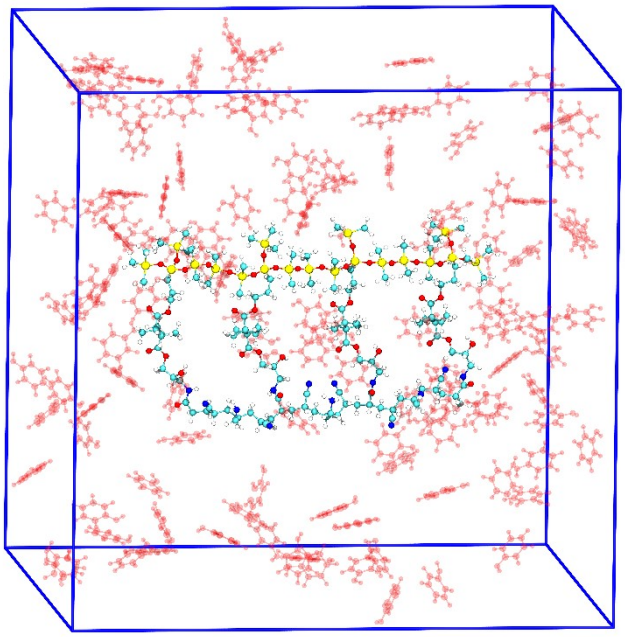

Fig. S28. The initial state of phenol adsorption at 9 wt% concentrations.

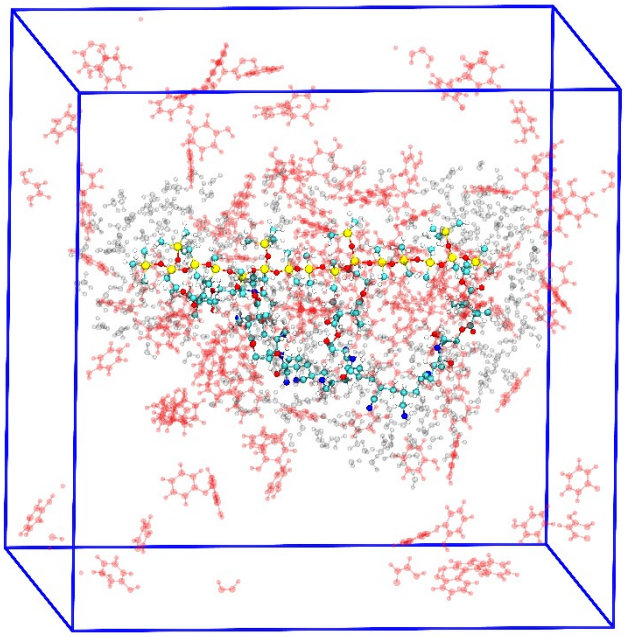

Fig. S29. The final state of phenol adsorption at 9 wt% concentrations.

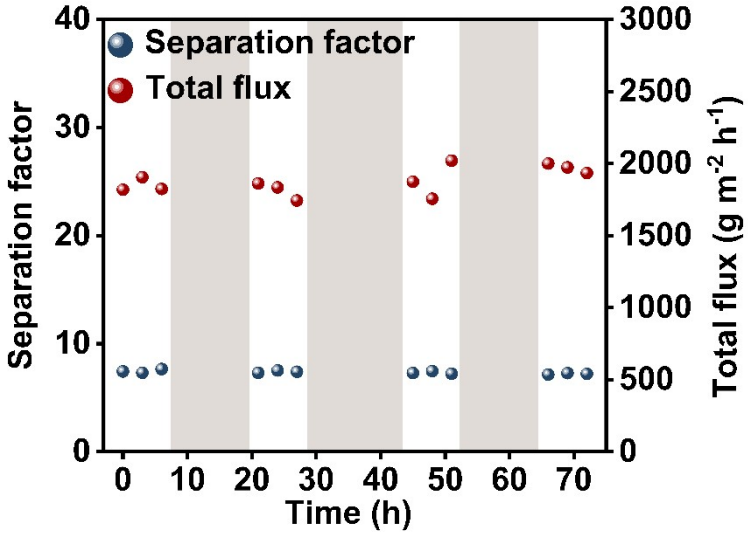

Fig. S30. PV stability test under extreme conditions of PDMS/GPAN-1 (20 wt%, 80 °C).

We also added a PV stability test under a higher concentration of 20 wt% than 6 wt%. Result shows that no significant degradation in separation performance observed throughout a 72 h of continuous operation, proving a stable separation towards phenol. Furthermore, the membrane's performance has no degradation after being removed and reused 3 times, demonstrating an excellent reusability. In fact, the membrane can be reused multiple times as long as it remains within the module[20].

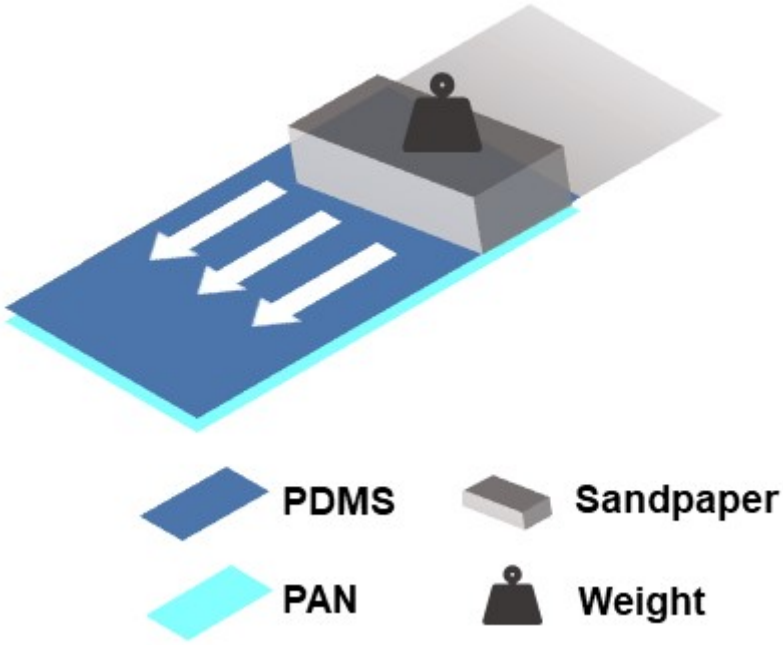

Fig. S31. Schematic diagram of friction experiment.

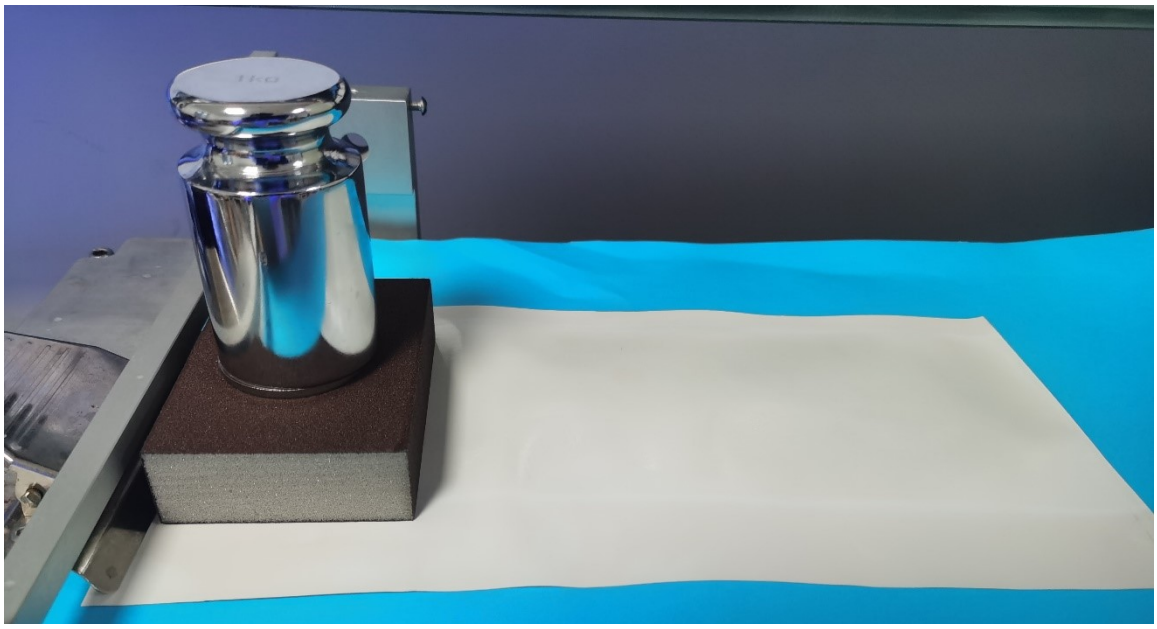

Fig. S32. Schematic diagram of self-designed friction experimental device.

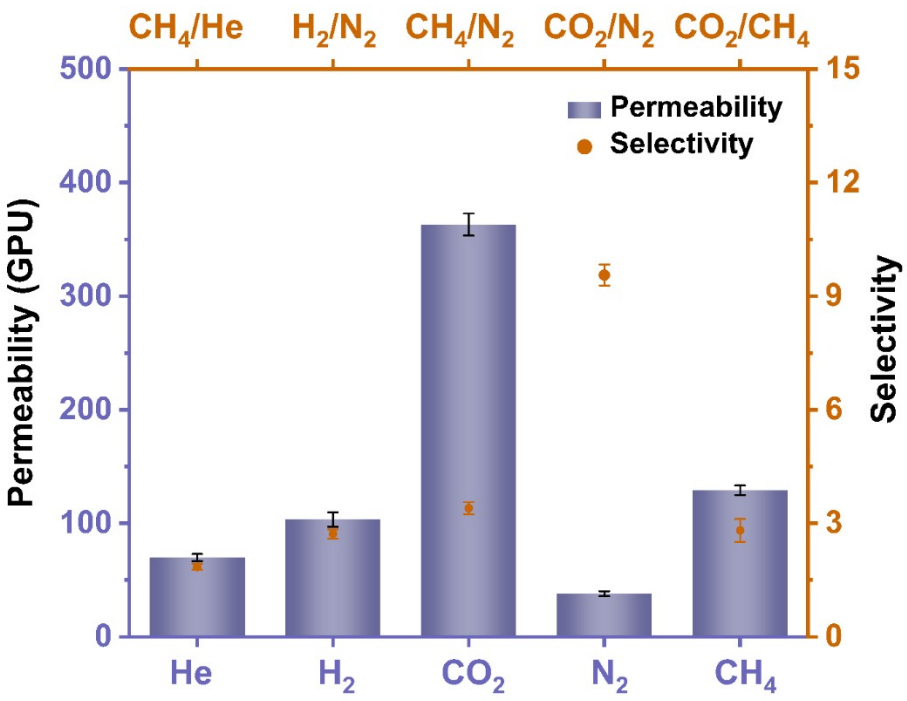

Fig. S33. Gas separation performance of PDMS/GPAN-1.

It shows the gas separation performance of the prepared PDMS/GPAN-1. The selectivity of CH_4/N_2 and CO_2/N_2 is 3.4 and 9.6 respectively, and the permeability of CO_2 and CH_4 is 363 and 129 GPU respectively, indicating strong separation ability of CH_4/N_2 and CO_2/N_2.

Table S4. Comparison of membranes of this work with previous reports in PV performance of phenol/water separation.

Membranes	Feed temp. (℃)	Phenol conc.(wt%)	Total flux ($g \cdot m^{-2} h^{-1}$)	Separation factor	Ref.
PDMS	50	0.2	1000	5	21
PDMS	50	0.1	800	6.5	21
PDMS	70	0.5	300	8.78	22
PDMS	70	0.5	230	6.7	22
PDMS	70	0.5	500	3	22
PDMS	60	0.5	310	5.4	22
PDMS	60	0.5	420	2.3	22
PEBA	60	0.5	327.6	6.3	23
PDMS	80	0.1	578	4.56	24
PDMS	40	0.1	800	3.3	24
PDMS	40	0.1	1100	2.7	24
PDMS	40	0.1	710	3.2	24
PDMS	40	0.2	1000	3	24
PDMS	30	0.1	600	3.2	24
PDMS	50	0.1	900	3.5	24
PU[a]	35	0.7	730	9	25
PEBA	70	0.8	846	39	26
PEBA	60	0.6	1011	36	27
PEBA	50	0.01	529	34	27
PDMS/GPAN-1	60	0.1	1245.6	9.54	This work

(a): polyurethane.

Table S5. Comparison of membrane-formation times with the reported PEBA membranes.

Membranes	Methods	Membrane-formation time	Ref.
PEBA	Thermal	24 h	26
PEBA	Thermal	48 h	27
PEBA	Thermal	24 h	28
PEBA	Thermal	24 h	29
PEBA	Thermal	24 h	30
PEBA	Thermal	12 h	31
PEBA	Thermal	24 h	32
PEBA	Thermal	24 h	33
PEBA	Thermal	24 h	34
PEBA	Thermal	12 h	35
PDMS/GPAN-1	UV	300 s	This work

10. References

1 H. Zhou, Y. Su, X. Chen, J. Luo, S. Tan and Y. Wan, *J. Membr. Sci.,* 2016, **520**, 779-789.

2 S. Li, P. Li, D. Cai, H. Shan, J. Zhao, Z. Wang, P. Qin and T. Tan, *J. Membr. Sci.,* 2019, **579**, 141-150.

3 M. K. Ghose, *Water Res.*, 2002, **36**, 1127-1134.

4 P. Sachan, S. Madan and A. Hussain, *Appl. Water Sci.*, 2019, **9**, 100-105.

5 L. Shao, T.-S. Chung, S. H. Goh and K. P. Pramoda, *J. Membr. Sci.,* 2005, **256**, 46-56.

6 M. Abedi, M. Sadeghi and M. Pourafshari Chenar, *J. Taiwan Inst. Chem. Eng.*, 2015, **55**, 42-48.

7 Í. G. M. d. Silva, E. F. Lucas and R. Advincula, *Sep. Purif. Technol.*, 2021, **278**, 119365-119376.

8 D. Cwikel, Q. Zhao, C. Liu, X. Su and A. Marmur, *Langmuir*, 2010, **26**, 15289-15294.

9 Y. Hang, G. Liu, K. Huang and W. Jin, *J. Membr. Sci.,* 2015, **494**, 205-215.

10 C. Liu, Z. Si, H. Wu, Y. Zhuang, C. Zhang, G. Zhang, X. Zhang and P. Qin, *Ind. Eng. Chem. Res.,* 2023, **3**, 1523-1532.

11 H. Zhu, Y. Pan, X. Sun, G. Liu, M. Qiu, X. Ding, Y. Fan and W. Jin, *J. Membr. Sci.,* 2021, **640**, 119835-119848.

12 Z. Dong, H. Zhu, Y. Hang, G. Liu and W. Jin, *Engineering,* 2020, **6**, 89-99.

13 Q. Li, L. Cheng, J. Shen, J. Shi, G. Chen, J. Zhao, J. Duan, G. Liu and W. Jin, *Sep. Purif. Technol.,* 2017, **178**, 105-112.

14 K. Huang, G. Liu, Y. Lou, Z. Dong, J. Shen and W. Jin, *Angew. Chem. Int. Ed.,* 2014, **53**, 6929-6932.

15 W. Wei, S. Xia, G. Liu, X. Gu, W. Jin and N. Xu, *AIChE J.,* 2010, **56**, 1584-1592.

16 Q. Liu, Y. Li, Q. Li, G. Liu, G. Liu and W. Jin, *Sep. Purif. Technol.,* 2019, **214**, 2-10.

17 F. M. Barton, *Chem. Rev.,* 1975, **75**, 731-753.

18 S. Mandal and V. G. Pangarkar, *Sep. Purif. Technol.,* 2003, **30**, 147-168.

19 J. Niemistö, W. Kujawski and R. L. Keiski, *J. Membr. Sci.*, 2013, **434**, 55-64.

20 G. Liu and W. Jin, *J. Membr. Sci.*, 2021, **636**, 119557-119587.

21 Bakhshi, T. Mohammadi and A. Aroujalian, *J. Appl. Polym.,* 2008, **107**, 1777-1782.

22 H. Ye, X. Yan, X. Zhang and W. Song, *Iran. Polym. J.,* 2017, **26**, 639-649.

23 K. W. Böddeker, G. Bengtson and E. Bode, *J. Membr. Sci.,* 1990, **53**, 143-158.

24 D. Li, J. Yao, H. Sun, B. Liu, S. van Agtmaal and C. Feng, *Appl. Surf. Sci.,* 2018, **427**, 288-297.

25 P. Shao and R. Y. M. Huang, *J. Membr. Sci.,* 2007, **287**, 162-179.

26 C. Ding, X. Zhang, C. Li, X. Hao, Y. Wang and G. Guan, *Sep. Purif. Technol.*, 2016, **166**, 252-261.

27 X. Cao, K. Wang and X. Feng, *J. Membr. Sci.*, 2021, **623**, 119043-119057.

28 X. Hao, M. Pritzker and X. Feng, *J. Membr. Sci.*, 2009, **335**, 96-102.

29 Y. X. Xue, F. F. Dai, Q. Yang, J. H. Chen, Q. J. Lin, L. J. Fang and W. W. Lin, *ACS Omega*, 2022, **7**, 23467-23478.

30 P. Cai, J. Li, D. Song, N. Zhang, N. Wang and Q.-F. An, *J. Membr. Sci.*, 2024, **695**, 122489-122498.

31 G. Mao, Y. Sheng, S. Ju, H. Zhou and W. Jin, *Sep. Purif. Technol.*, 2024, **337**, 126406-126413.

32 Z. Zhang, E. Gou, Z. Zhao and J. Yao, *Sep. Purif. Technol.*, 2023, **327**, 124900-124913.

33 P. Cai, J. Li, N. Zhang, D. Song, N. Wang and Q.-F. An, *J. Membr. Sci.*, 2023, **668**, 121254-121263.

34 L. J. Fang, J. H. Chen, Q. Yang, W. W. Lin, Q. J. Lin, Y. S. He and Y. Z. Zhuo, *J. Taiwan Inst. Chem. Eng.*, 2022, **134**, 104356-104364.

35 M. Sheikh, M. Asghari and M. Afsari, *Alexandria Eng. J.*, 2018, **57**, 3661-3669.